Chapter 2
Nitriding of Binary Iron-Based Alloys: An Overview

Abstract Nitrided iron-based alloys are widely used in various industrial applications. Composition of such alloys is one of the factors in governing their nitriding behavior. This chapter reviews some of the interesting results associated with nitrided binary iron-based alloys. It was observed that the concentration of alloying elements influenced the precipitation morphologies in nitrided zone of Fe–Cr and Fe–V alloys. Nitrided zone of such binary alloys showed the presence of "excess nitrogen" (i.e., actual nitrogen content was more than the normal/expected nitrogen content). The occurrence of excess nitrogen was explained by using nitrogen absorption isotherms and kinetics of nitriding studies. The results obtained for the nitrided Fe-7 wt%Cr and Fe-4 wt%V alloys suggested that the compound layer, which appears "white" under optical microscope, was not just a pure γ'-Fe_4N, but was a combination of γ' plus nitrides of alloying element.

Keywords Fe–Cr alloy · Fe–V alloy · Nitriding · Discontinuous precipitation

2.1 Introduction

Nitriding of iron-based alloys is widely practiced in industries to enhance fatigue, wear, and anticorrosion properties of engineering components. The nitriding alloys used for these applications contain many alloying elements. Therefore, it is difficult to understand the nitriding behavior of the alloys caused by a particular alloying element. In this regard, a sequential study of nitriding of pure iron, binary alloys, etc., could be useful. Information about nitriding of pure iron is provided in detail in Refs. [1, 2]. A systematic understanding of the nitriding behavior of iron-based alloys has evolved over many years due to research by various authors, for example, see Refs. [3–5] for nitriding of Fe–Ti alloys, Refs. [6–12] for nitriding of Fe–Al alloys, Refs. [13–22] for nitriding of Fe–V alloys, Refs. [23–27] for nitriding of Fe–Cr alloys, and Refs. [28, 29] for nitriding of ternary alloys. Some of the interesting phenomena for nitriding of binary iron-based alloys, especially, Fe–Cr and Fe–V alloys, are summarized in this chapter.

S. S. Hosmani et al., *An Introduction to Surface Alloying of Metals*,
SpringerBriefs in Manufacturing and Surface Engineering,
DOI: 10.1007/978-81-322-1889-0_2,

2.2 Precipitation Morphologies in Nitrided Fe–Me Alloys

Nitriding of Fe-based alloys is generally carried out in the temperature range of 500–600 °C. During nitriding of the alloy, the surface of the specimen achieves equilibrium with the nitriding atmosphere and nitrogen dissolution in the ferrite (α-Fe) occurs. Dissolved nitrogen starts diffusing in the ferrite. Interaction of nitride forming alloying element with diffusing nitrogen leads to the formation of nitride precipitate. Precipitation of nitride in the ferrite matrix needs to overcome the activation energy barrier for nucleation. Morphology of the precipitate depends on the precipitate–matrix interface energy and lattice or volume misfit strain energy. For small misfit, the total change in free energy of the system is smaller for coherent/semi-coherent precipitates than incoherent precipitates. However, as precipitate size increases, incoherent precipitate could be associated with smaller free energy change of the system than coherent/semi-coherent precipitates [30]. In other words, the driving force for precipitate coarsening is the decrease in free energy of the system caused by the decrease in total precipitate–matrix interface area (for a constant volume fraction of the precipitates before and after coarsening) and misfit strain energy. Such coarsening is associated with decrease in the hardness of the alloy.

Nitrided Fe–Cr and Fe–V alloys showed two types of precipitation morphologies: (i) continuous precipitation and (ii) discontinuous precipitation.

These precipitations are defined as follows: (i) Continuous precipitation involves the transport of atoms to the growing nuclei of precipitating phase in the supersaturated matrix. This transport (diffusion) of atoms occurs over relatively large distances in the parent phase (i.e., long-range diffusional process). During this process, the average composition of the parent phase changes continuously toward its equilibrium concentration. (ii) Discontinuous precipitation involves structural and compositional changes in the region immediately adjacent to the advancing precipitate–matrix interface. In this precipitation, the composition of parent phase remains unchanged until it is consumed by the advancing precipitate–matrix interface.

Light optical micrographs of nitrided Fe-7 wt%Cr and Fe-4 wt%V alloys are shown in Figs. 2.1 and 2.2. Two types of the grains/regions are observed in the nitrided region—bright and dark. The bright region is adjacent to the non-nitrided core. However, the surface region is fully occupied by the dark grains. Micrographs are useful in understanding the possible sequence of events at a particular depth during the growth of nitrided zone. The sequence of events could be as follows: nontreated core → bright region → dark region. This suggests that the formation of bright region occurs initially which later transforms into dark region. Interestingly, the formation of dark region in the nitrided zone of Fe–Cr and Fe–V alloys depends on the concentration of alloying elements. Formation of dark region in the nitrided zone does not occur in the alloys containing up to 1 wt%Cr in case of Fe–Cr alloys (see Fig. 2.2) and 2 wt%V in case of Fe–V alloys (see Figs. 2.1 and 2.3). Nitriding for long duration does not transform bright region into

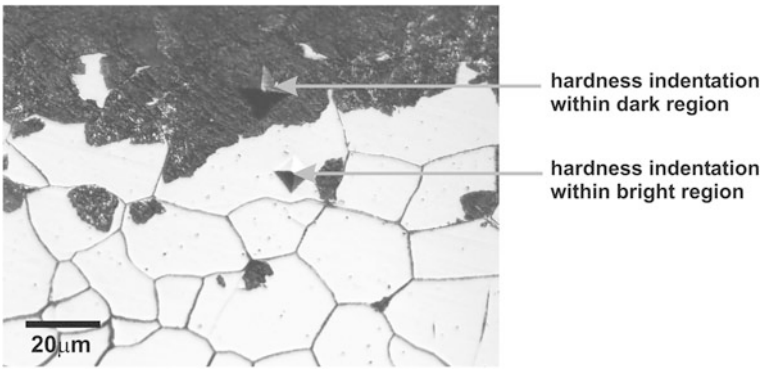

Fig. 2.1 Optical micrograph showing two hardness indentations (performed with the same load) in one original grain of the thick nitrided Fe-4 wt%V alloy: the *dark* region of the grain exhibits a larger indentation (i.e., possesses lower hardness) than the *bright* part of the grain. (Reprinted from Hosmani et al. [21], with permission from Elsevier)

dark region in the nitrided Fe-1 wt%Cr and Fe-2 wt%V alloys. These results suggest that high concentration of alloying elements promotes the formation of dark region in the nitrided zone. This is confirmed by using scanning electron microscopy (SEM), in Refs. [21, 24], where the dark region has lamellar morphology. However, optical microscopy and SEM are incapable to reveal any precipitation morphology in the bright region. X-ray diffraction studies [21, 24] have confirmed that the dark region consists of α-Fe and alloying-element-nitride phase (i.e., CrN and VN in nitrided Fe–Cr and Fe–V alloys, respectively). However, transmission electron microscopy studies [18, 31] have confirmed the presence of nitride precipitates in the bright region. Dark grains have considerably lower hardness than bright grains as demonstrated by the microhardness measurements (Figs. 2.1, 2.2, 2.3). On the basis of observed results, the bright region was designated as "continuous" precipitated region and dark region was designated as "discontinuous" coarsened region.

The mechanism for the discontinuous coarsening in nitrided Fe–V and Fe–Cr alloys is explained in Refs. [21, 24]. The essence of this mechanism is summarized below.

During nitriding, diffusing nitrogen interacts with vanadium (in Fe–V alloys) or chromium (in Fe–Cr alloys). This interaction initially leads to the formation of vanadium nitride or chromium nitride precipitates which are finely dispersed in α-Fe (ferrite) matrix ("continuous" precipitation). These precipitates are in the form of platelets (e.g., plate-like precipitates of VN are typically about 40 Å long with thickness of about 10 Å) which are probably coherent/semi-coherent with the α-Fe matrix [18, 31]. The lattice parameters of VN, CrN, and α-Fe are 0.4137, 0.4149, and 0.2866 nm, respectively. Due to the difference in lattice parameters of nitride and ferrite, the misfit-induced stress fields associated with the precipitates [18] are responsible for the high hardness values associated with "continuous" precipitated

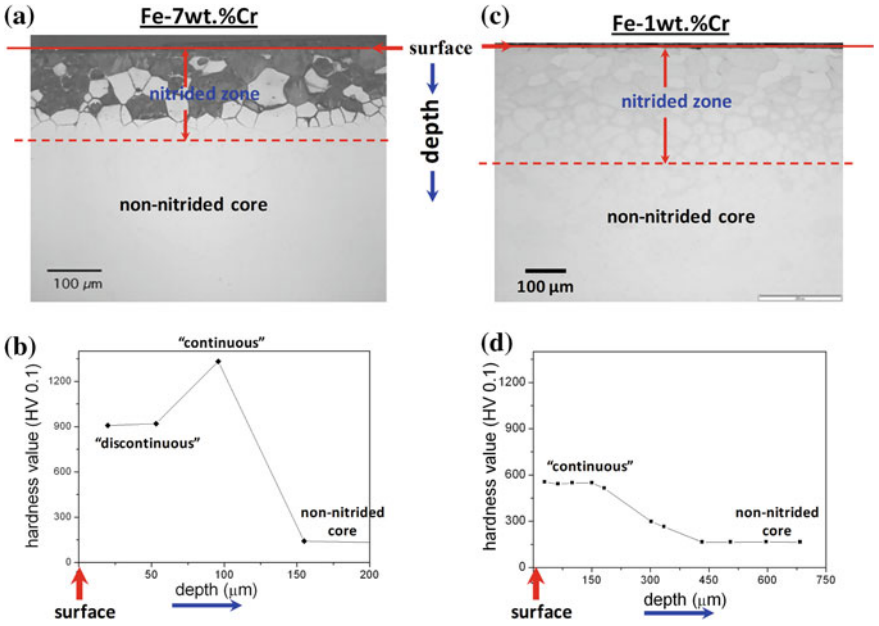

Fig. 2.2 Optical micrograph and corresponding microhardness-depth profile for **a** Fe-7 wt%Cr specimen nitrided at 580 °C for 4 h at a nitriding potential of 0.16 $atm^{-1/2}$ and **b** Fe-1 wt%Cr specimen nitrided at 580 °C for 5 h at a nitriding potential of 0.10 $atm^{-1/2}$

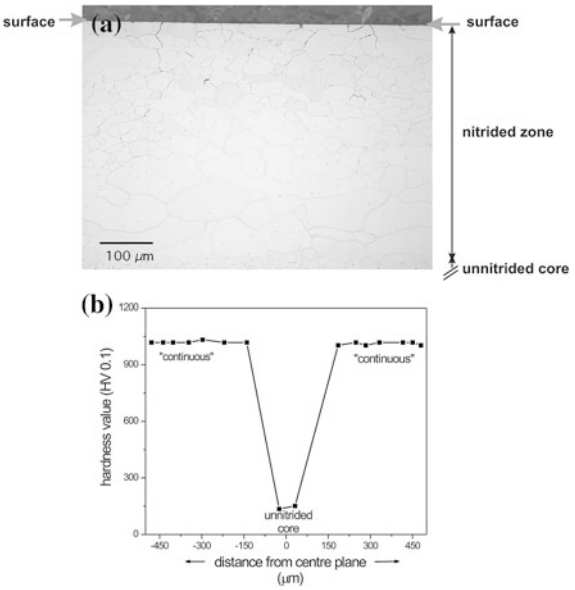

Fig. 2.3 **a** Light optical micrograph of the etched cross-section of the thick (thickness of 1.0 mm) Fe-2 wt%V specimen nitrided at 580 °C for 10 h at a nitriding potential of 0.10 $atm^{-1/2}$. **b** Hardness-depth profile of the same specimen. (Reprinted from Hosmani et al. [21], with permission from Elsevier)

region (i.e., bright region of optical micrograph). A coarsening of the nitride precipitates occurs during prolonged nitriding treatment. The driving force for coarsening is the reduction in Gibbs free-energy caused by relaxation of internal long-range stress fields and reduction of precipitate–matrix interfacial area. This coarsening in general could be continuous growth of the precipitates ("Ostwald ripening"), but for the Fe–V and Fe–Cr alloys containing high concentration of alloying elements, coarsening occurs by a "discontinuous coarsening" of the former continuous precipitates. This discontinuous coarsening involves the growth of α-Fe and VN lamellae from nucleation sites like surfaces and grain boundaries. The following reaction possibly operates during discontinuous coarsening of nitride precipitates:

$$\alpha^{|} + \beta^{|} \rightarrow \alpha + \beta \tag{2.1}$$

where $\beta^{|}$ denotes coherent nitride precipitates in a supersaturated (with nitrogen) ferrite matrix ($\alpha^{|}$). The reaction consists of replacing the submicroscopical and coherent/semi-coherent nitride precipitates by nitride lamellae ($\beta^{|} \rightarrow \beta$) with simultaneous elimination of the nitrogen supersaturation of the ferrite matrix ($\alpha^{|} \rightarrow \alpha$).

Therefore, on nitriding of Fe–V and Fe–Cr alloys that contain high concentrations of alloying elements, the following two reaction fronts can be expected: (i) initially, inward diffusion of nitrogen and the reaction of alloying element with N to form finely dispersed coherent/semi-coherent nitride precipitates and then (ii) subsequent discontinuous coarsening of the former continuous precipitates (see Figs. 2.1 and 2.2). As mentioned above, the hardness of showing discontinuous precipitated region is significantly lower than that of the continuous precipitated region. This behavior is a direct consequence of coarsening with associated loss of coherency. The larger the concentration of alloying element in the alloy, the larger the volume fraction of the nitride precipitates in the ferrite matrix. Therefore, the driving force for the discontinuous coarsening reaction will be larger for alloys containing higher concentration of alloying element. This concept explains the presence of dark region in nitrided Fe-4 wt%V alloy, but the absence of such region in nitrided Fe-2 wt%V alloy. Similar nitriding behavior in Fe–Cr alloys is observed.

It must be noted that the above-mentioned continuous and discontinuous precipitation morphologies are not reported in the literature for nitrided Fe–Ti [3–5] and Fe–Al [6–12] alloys.

2.3 Excess Nitrogen

The phenomenon of "excess nitrogen" in nitrided iron-based alloys was introduced in Chap. 1. The quantity of "excess nitrogen" is the difference between actual (experimental) nitrogen content and expected (theoretical) nitrogen content in the

nitrided alloys. Expected nitrogen content in the nitrided Fe–Me (Me = Cr/V/Al/Ti) alloy is summation of the nitrogen necessary for precipitation of all alloying elements as nitride, $[N]_{MeN_n}$, and equilibrium saturation of nitrogen in the unstrained ferrite matrix, $[N]_{\alpha}^{0}$, at the given nitriding temperature and nitriding potential.

The total amount of nitrogen absorbed by the alloy is summation of various types of nitrogen. These types of nitrogen can be understood by using nitrogen absorption isotherm [7, 22, 32], which shows the dependence of the amount of nitrogen taken up by a (homogeneously) nitrided specimen as a function of the nitriding potential (directly related to the chemical potential of the nitriding atmosphere) [22]. Nitrogen uptake is determined by weight measurements of the specimens before and after the treatments. This method involves the following major steps:

(i) *Pre-nitriding*: this involves nitriding of the foil specimen such that complete thickness of the specimen is homogeneously nitrided.
(ii) *De-nitriding*: After pre-nitriding, the specimen is de-nitrided in pure H_2 at lower temperature than pre-nitriding temperatures. De-nitriding removes all types of nitrogen present in the specimen except the nitrogen which is strongly bonded to alloying element to form nitride phase.
(iii) *Determination of nitrogen absorption isotherms*: After the consecutive pre- and de-nitriding treatments, nitrogen absorption isotherms are determined at temperatures below the pre-nitriding temperature. Lower temperatures are selected to avoid any change in the precipitation morphology.

Nitrogen content in pre- and de-nitrided Fe-1.04 at.%Cr specimens are shown in Fig. 2.4. The difference between nitrogen content in pre-nitrided specimen and normal nitrogen uptake is the "total excess nitrogen." Figure 2.5 shows the nitrogen absorption isotherms for pre- and de-nitrided Fe-1.04 at.%Cr specimens at 560 °C and at 530 °C. Total nitrogen uptake in the nitrided specimen can be broadly classified into three types (I, II, and III) of nitrogen [7, 22, 32]:

(i) Type I: This is the strongly bonded nitrogen to alloying element in the corresponding stoichiometric nitride phase. This nitrogen cannot be removed easily by de-nitriding in a pure H_2 atmosphere. Type I nitrogen is indicated by level "A" in Fig. 2.5.
(ii) Type II: This is the adsorbed nitrogen at the nitride/matrix interface. This nitrogen is less strongly bonded compared to type I nitrogen. Therefore, this nitrogen can be removed by de-nitriding. Type II nitrogen is called *immobile excess nitrogen* because it does not take part in growth kinetics of the diffusion zone. This nitrogen corresponds to the difference between levels "B" and "A" in Fig. 2.5.
(iii) Type III: This is the dissolved nitrogen in the octahedral interstices of the ferrite matrix surrounding the precipitates. Type III nitrogen can be removed easily by de-nitriding. The amount of dissolved nitrogen in the ferrite matrix is directly proportional to the nitriding potential. Therefore, the straight-line dependence above level "B" in Fig. 2.5 represents the nitrogen dissolved

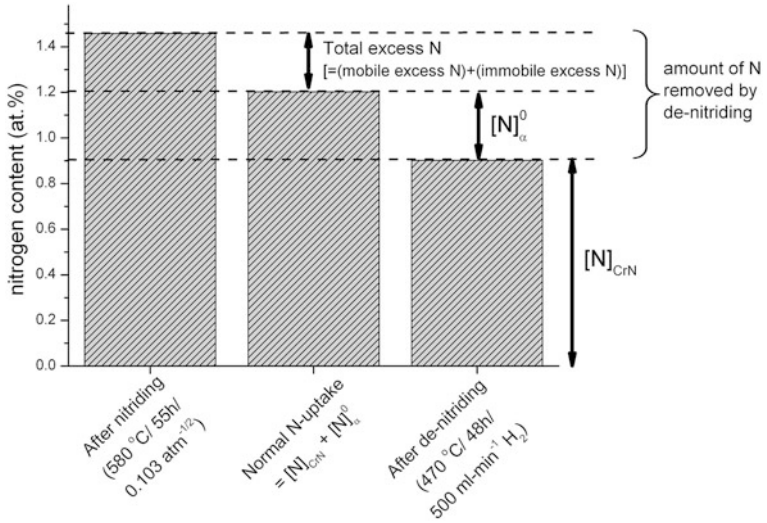

Fig. 2.4 Summary of the pre-nitriding (55 h at 580 °C and $r_n = 0.10$ atm$^{-1/2}$) and de-nitriding (48 h at 470 °C in pure H_2) experiments performed with Fe-1.04 at.%Cr foil specimens (thickness of 0.2 mm). $[N]_{CrN}$ is the amount of nitrogen required for the precipitation of all Cr as CrN and $[N]^0_\alpha$ is the amount of nitrogen dissolved in an unstrained ferrite matrix at the pre-nitriding conditions. (Reprinted from Hosmani et al. [32], with permission from Springer)

interstitially in the ferrite matrix. However, there is a difference between the nitrogen uptake in ferrite of nitrided alloy and unstrained pure iron. Higher nitrogen uptake in the ferrite of nitrided alloy is due to the presence of strain, which is caused by the misfit between nitride precipitate and ferrite matrix. $[N]_{strain}$ is also called *mobile excess nitrogen* because it diffuses to give excess thickness to the nitrided zone.

Interestingly, nitrogen content in the nitrided zone of Fe-4 wt%V alloy depends on the type of precipitation morphology [21]. Figure 2.6 shows the elemental concentration-depth profiles of the nitrided layer of the nitrided Fe-4 wt%V specimen. The presence of excess nitrogen in the nitrided zone is evident. Nitrogen content at the location of discontinuously transformed regions/grains is significantly lower than the continuously transformed regions/grains. In other words, the discontinuous transformation in nitrided Fe-4 wt%V alloy is associated with the loss in capacity of excess nitrogen. However, the nitrogen uptake in the nitrided zone of Fe–Cr alloys (containing 4, 7, 13, 20 wt%Cr) is independent of discontinuous or continuous precipitated regions [24–26]. The nitrogen-absorption isotherm for the discontinuously transformed Fe-20 wt%Cr alloy showed the presence of excess nitrogen in the nitrided specimen [27], i.e., the coarse and lamellar precipitation morphology of CrN/α-Fe is associated with considerable quantity of excess nitrogen. This excess nitrogen could be ascribed to an unexpected, minor fraction of the total Cr content in the alloy present as coherent, tiny nitride platelets within the ferrite

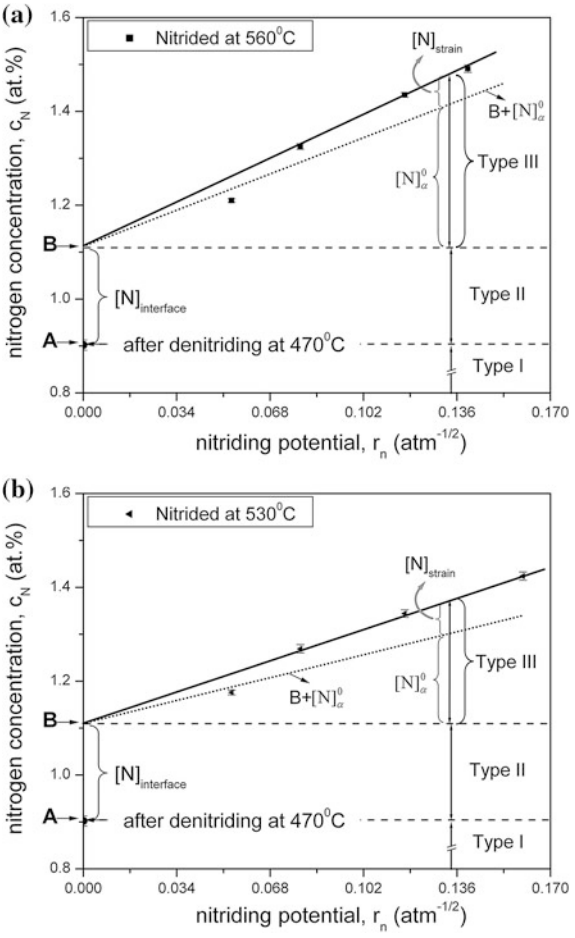

Fig. 2.5 Nitrogen-absorption isotherms as observed for pre- and de-nitrided Fe-1.04 at.%Cr specimens **a** at 560 °C and **b** at 530 °C. The nitrogen level after de-nitriding is indicated by "A." The linear portion of the absorption isotherm is indicated by the *solid line* that intersects the ordinate at $r_n = 0$ at a nitrogen level indicated by "B." Level B plus the nitrogen solubility in unstrained ferrite is shown by the *dotted line*. The lattice solubilities of nitrogen in pure iron, $[N]_\alpha^0$, as function of the nitriding potential at 560 and 530 °C were taken from Ref. [22]. (Reprinted from Hosmani et al. [32], with permission from Springer)

lamellae of the "discontinuously coarsened" lamellar precipitation morphology, as evidenced by transmission electron microscopy [27].

Nitriding kinetics study [21, 25] is also useful to understand the occurrence of excess nitrogen in nitrided alloys. By using the simple model originally proposed for "internal oxidation" (see Chap. 1), expected nitriding depth can be calculated. Experimental values for nitriding depth and total excess nitrogen can be obtained from electron probe microanalyzer (EPMA). Incorporating experimental nitriding depth in the model gives actual nitrogen content in the ferrite matrix at specimen surface. Difference between such obtained nitrogen content and the nitrogen in unstrained ferrite (calculated from Refs. [1, 2]) gives the *mobile excess nitrogen* content. Subtracting mobile excess nitrogen from total excess nitrogen gives *immobile excess nitrogen* content. Such calculations are summarized in Table 2.1 for nitrided Fe-4 wt%V and Fe-2 wt%V alloys [21]. In this way, the total amount of excess nitrogen can be divided into mobile and immobile excess nitrogen.

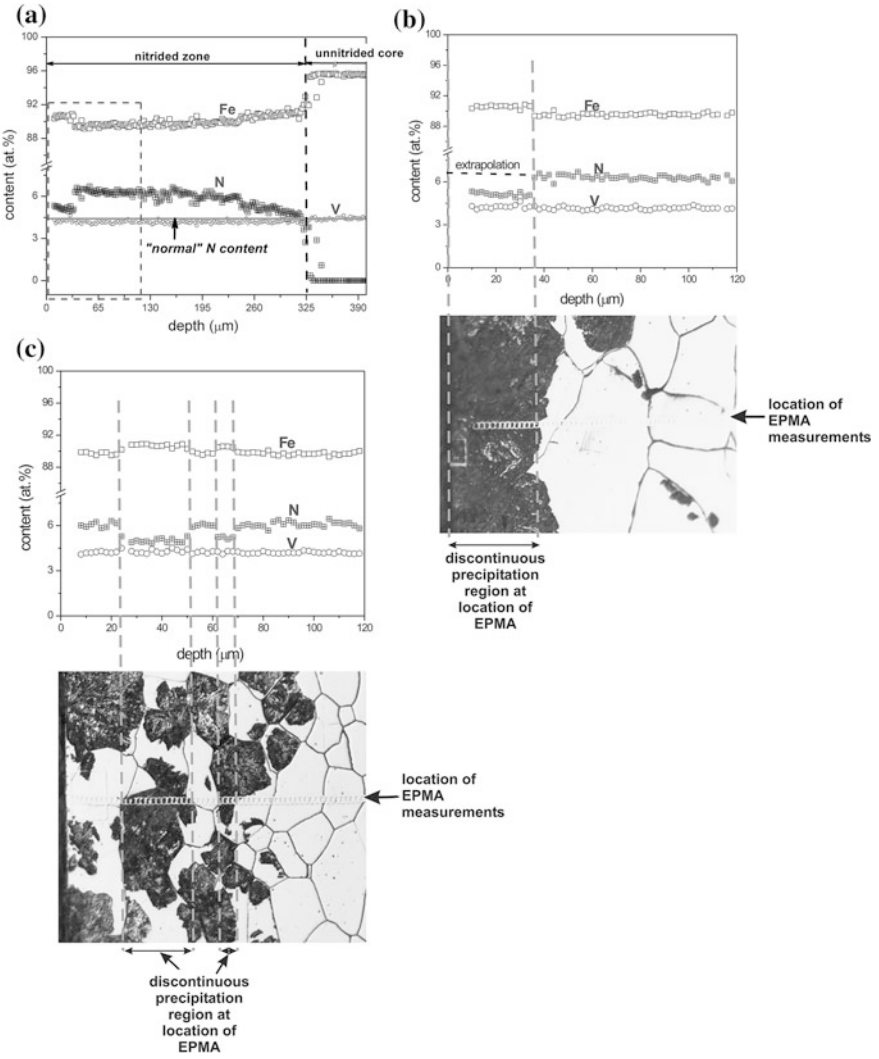

Fig. 2.6 **a** Elemental (N, V, Fe) concentration-depth profiles of Fe-4 wt%V alloy nitrided at 580 °C for 10 h at a nitriding potential of 0.10 $atm^{-1/2}$. The horizontal *gray line* indicates the "normal" amount of nitrogen uptake. **b** Enlargement of part of the depth profile, indicated by the *dashed rectangle* in (**a**), together with the light optical micrograph of the cross-section analyzed (which was etched after EPMA analysis) showing the location of the EPMA measurements (as revealed by the usual track of carbon contamination). Clearly, the nitrogen concentration in the surface adjacent *dark* part of the nitrided zone is smaller than in the *bright* part of the nitrided zone. **c** Part of elemental concentration-depth profile recorded at another location of the same specimen, together with the light optical micrograph of the cross-section analyzed (which was etched after EPMA analysis) showing the location of the EPMA measurements. Clearly, the nitrogen concentration at the location of *dark* grains ("discontinuously" transformed grains) is smaller than in the *bright* grains ("continuously" precipitated grains). (Reprinted from Hosmani et al. [21], with permission from Elsevier)

Table 2.1 Tabular presentation of the expected nitriding depth calculated using "internal oxidation" model (see Chap. 1) with $c^{S}_{N_\alpha} = c^{S,0}_{N_\alpha}$, the measured nitriding depth determined from the experimental (EPMA) data, the total amount of excess nitrogen at the surface determined from EPMA, the equilibrium nitrogen content in (stress-free) α-Fe ($c^{S,0}_{N_\alpha}$), the nitrogen content in α-Fe at the surface calculated using "internal oxidation" model with experimental values for the nitriding depths ($c^{S}_{N_\alpha}$), the amount of dissolved, mobile excess nitrogen ($=c^{S}_{N_\alpha} - c^{S,0}_{N_\alpha}$), and the amount of immobile (adsorbed at precipitate /matrix interfaces) excess nitrogen

		Fe-4 wt%V	Fe-2 wt%V
(1)	Expected nitriding depth ("internal oxidation" model with $c^{S}_{N_\alpha} = c^{S,0}_{N_\alpha}$) (μm)	210	296
(2)	Measured nitriding depth (experimental (EPMA) results) (μm)	322	425
(3)	Total excess nitrogen at surface (measured from EPMA) (at.%)	2.31[a]	1.15
(4)	Equilibrium nitrogen content in α-Fe, $c^{S,0}_{N_\alpha}$ (calculated from Refs. [1, 2]) (at.%)	0.24	0.24
(5)	Nitrogen content in α-Fe at the surface, $c^{S}_{N_\alpha}$ ("internal oxidation" model with experimental values for nitriding depths) (at.%)	0.56	0.49
(6) = (5) − (4)	Dissolved (i.e., mobile) excess nitrogen ($=c^{S}_{N_\alpha} - c^{S,0}_{N_\alpha}$) (at.%)	0.32	0.25
(7) = (3) − (6)	Adsorbed precipitate/matrix interfacial (i.e., immobile) excess nitrogen (at.%)	1.99	0.91

All results have been given for the Fe-4 wt% V and Fe-2 wt% V alloys, nitrided at 580 °C for 10 h at a nitriding potential of 0.10 $atm^{-1/2}$. (Reprinted from Hosmani et al. [21], with permission from Elsevier)

[a] Estimate; see Ref. [21]

2.4 Compound-Layer Formation

In nitriding, compound-layer is also known as whiter-layer. Compound-layer can be made up of γ′-Fe_4N and/or ε-Fe_3N. Compound-layer formation over Fe-based alloys depends on the chosen nitriding parameters, like temperature and nitriding potential. At a given nitriding temperature, the formation of compound-layer can be controlled by selecting appropriate nitriding parameters. Effect of nitriding potential on nitriding kinetics of Fe-7 wt%Cr was investigated at constant temperature (580 °C) and time (4 h) [26]. The Fe-7 wt%Cr specimens nitrided at low nitriding potentials ($r_n = 0.01–0.16$ $atm^{-1/2}$) do not show compound-layer formation. However, at high nitriding potentials ($r_n = 0.21–0.82$ $atm^{-1/2}$), γ′-Fe_4N layer formation occurs. The nitriding potential has great influence on the depth of the nitrided zone. The nitriding depth depends approximately linearly on the square root of the nitriding potential for the specimens nitrided in the range of nitriding potentials of 0.01–0.16 $atm^{-1/2}$. As soon as a closed iron-nitride layer forms on the surface, the dependence of the nitriding kinetics on the nitriding potential becomes marginal. At constant temperature and time, growth kinetics of

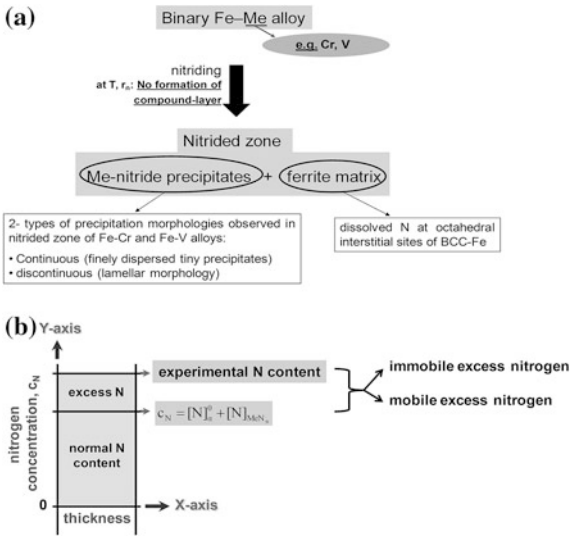

Fig. 2.7 Summary of the important aspects of the nitriding behavior of Fe–Cr and Fe–V alloys

the diffusion zone is dependent on the solubility of nitrogen in ferrite matrix at the specimen surface. Once there is a formation of compound-layer on the specimen surface, the amount of nitrogen dissolved in the ferrite matrix at the interface between compound-layer and diffusion zone becomes independent of nitriding potential. The growth of compound-layer with nitriding potential is insignificant. Therefore, the overall nitriding depth (diffusion zone plus compound-layer thickness) becomes independent of nitriding potential once the compound-layer forms on the specimen's Fe-7 wt%Cr surface.

Nonuniform thickness and irregular penetration of the compound-layer in the diffusion zone are observed for nitrided Fe-7 wt%Cr and Fe-4 wt%V alloys [33, 34]. Phase analysis (by using x-ray diffraction) and quantitative analysis (by using electron probe microanalysis) of the compound-layer demonstrated the presence of alloying element nitride phase within γ'-Fe_4N matrix [33, 34]. These findings for nitrided Fe–Cr and Fe–V alloys suggest that the compound-layer, which appears "white" under optical microscope, is not just a pure γ', but is a combination of γ' plus nitrides of alloying element.

2.5 Conclusions

- Important aspects of the nitriding behavior of Fe–Cr and Fe–V alloys are summarized in the form of a flowchart in Fig. 2.7.
- Nitriding of Fe–Cr and Fe–V alloys showed two types of nitride precipitation morphologies in the diffusion zone: continuous and discontinuous. The discontinuously precipitated region appears dark under optical microscope and has

lamellar morphology. Discontinuous precipitation depends on the concentration of alloying elements. This precipitation morphology is observed for nitrided alloys containing high concentration of alloying elements (more than about 2 wt% of alloying elements). However, these precipitation morphologies are not reported in the literature for nitrided Fe–Ti and Fe–Al alloys.

- Nitrided Fe–Me (Me = Cr/V/Al/Ti) alloys show the presence of excess nitrogen in the nitrided zone. Excess nitrogen can be well understood by using nitrogen absorption isotherms. Nitriding kinetics study is also useful to understand the occurrence of excess nitrogen in nitrided specimens. It has been realized that the total amount of excess nitrogen is the combination of two types of excess nitrogen: mobile and immobile. Mobile excess nitrogen is responsible for greater nitriding depth than the expected value.
- White-layer formed on the surface of nitrided Fe-7 wt%Cr and Fe-4 wt%V alloys has nonuniform thickness and consists of alloying element nitride phase within γ'-Fe_4N matrix.

References

1. Mittemeijer EJ, Slycke JT (1996) Chemical potentials and activities of nitrogen and carbon imposed by gaseous nitriding and carburizing atmospheres. Surf Eng 12:152–162
2. Mittemeijer EJ, Somers MAJ (1997) Thermodynamics, kinetics, and process control of nitriding. Surf Eng 13:483–497
3. Jack DH (1976) Acta Metall 24:137
4. Podgurski HH, Davis FN (1981) Acta Metall 29:1
5. Rickerby DS, Henderson S, Hendry A, Jack KH (1986) Acta Metall 34:1687
6. Podgurski HH, Oriani RA, Davis NA (1969) Trans Metall Soc AIME 245:1603 (with Appendix by Li JCM, Chou YT)
7. Biglari MH, Brakman CM, Mittemeijer EJ, van der Zwaag S (1995) Phil Mag 72A:931
8. Biglari MH, Brakman CM, Somers MAJ, Sloof WG, Mittemeijer EJ (1993) Z Metallkd 84:124
9. Steenaert JS, Biglari MH, Brakman CM, Mittemeijer EJ, van der Zwaag S (1995) Z Metallkd 86:700
10. Biglari MH, Brakman CM, Mittemeijer EJ, van der Zwaag S (1995) Metall Mater Trans 26A:765
11. Biglari MH, Brakman CM, Mittemeijer EJ (1995) Phil Mag 72A:1281
12. Meka S, Hosmani SS, Clauss AR, Mittemeijer EJ (2008) Int J Mater Res 99:808
13. Philipps A, Seybolt AU (1968) Trans Metall Soc AIME 242:2415
14. Pope M, Grieveson P, Jack KH (1973) Scand J Metall 2:29
15. Welch WD, Carpenter SH (1973) Acta Metall 21:1169
16. Krawitz A (1977) Scr Metall 11:117
17. Yang MM, Krawitz AD (1984) Metall Trans 15A:1545
18. Bor TC, Kempen ATW, Tichelaar FD, Mittemeijer EJ, van der Giessen E (2002) Phil Mag 82A:971
19. Djeghlal ME, Barrallier L (2003) Ann Chim Sci Mat 28:43
20. Gouné M, Belmonte T, Redjaimia A, Weisbecker P, Fiorani JM, Michel H (2003) Mater Sci Eng 351A:23
21. Hosmani SS, Schacherl RE, Mittemeijer EJ (2005) Acta Mater 53:2069
22. Hosmani SS, Schacherl RE, Mittemeijer EJ (2006) Acta Mater 54:2783

23. Hekker PM, Rozendaal HCF, Mittemeijer EJ (1985) J Mater Sci 20:718
24. Schacherl RE, Graat PCJ, Mittemeijer EJ (2002) Z Metalld 93:468
25. Schacherl RE, Graat PCJ, Mittemeijer EJ (2004) Metall Mater Trans A 35:3387
26. Hosmani SS, Schacherl RE, Mittemeijer EJ (2005) Mater Sci Technol 21:113
27. Hosmani SS, Schacherl RE, Lityńska-Dobrzyńska L, Mittemeijer EJ (2008) Phil Mag 88:2411
28. Clauss AR, Bischoff E, Hosmani SS, Schacherl RE, Mittemeijer EJ (2009) Metall Mater Trans 40A:1923
29. Jung KS, Schacherl RE, Bischoff E, Mittemeijer EJ (2010) Surf Coat Technol 204:1942
30. Porter DA, Easterling KE (1981) Phase transformations in Metals and alloys. Chapman & Hall, London
31. Vives Díaz NE, Hosmani SS, Schacherl RE, Mittemeijer EJ (2008) Acta Mater 56:4137–4149
32. Hosmani SS, Schacherl RE, Mittemeijer EJ (2008) J Mater Sci 43:2618–2624
33. Hosmani SS, Schacherl RE, Mittemeijer EJ (2006) Int J Mater Res (formerly Zeitschrift für Metallkunde) 97:1545–1549
34. Hosmani SS, Schacherl RE, Mittemeijer EJ (2009) J Mater Sci 44:520–527

Springer

http://www.springer.com/978-81-322-1888-3

An Introduction to Surface Alloying of Metals

Hosmani, S.; Kuppusami, P.; Goyal, R.K.

2014, XI, 133 p. 70 illus., Softcover
ISBN: 978-81-322-1888-3